Supporting Online Material

High resolution electroluminescent imaging of pressure distribution using a piezoelectric nanowire-LED array

Caofeng Pan[1,2], Lin Dong[1,2], Guang Zhu[1], Simiao Niu[1], Ruomeng Yu[1], Qing Yang[1], Ying Liu[1],

Zhong Lin Wang[1,2]*

1. School of Materials Science and Engineering, Georgia Institute of Technology, Atlanta, GA 30332-0245, USA

2. Beijing Institute of Nanoenergy and Nanosystems, Chinese Academy of Sciences, Beijing, 100085, P.R. China

*To whom the correspondence should be addressed. Email: zhong.wang@mse.gatech.edu

Contents:

A: Experiment set-up and measurement system

The measurement system was built based on an inverted microscope (Nikon Ti-E), 3D micromanipulation stages and a piezo nanopositioning stage (PI, P-753K078) with closed loop resolution 0.2 nm, as shown in Fig. S1. A normal force/pressure was applied on the NW LEDs by using a sapphire substrate with a convex character pattern of "PIEZO" molded on it at the first place. By controlling the 3D micromanipulation stages and the piezo nanopositioning stage, the pressure could be applied step by step at a fixed value. The detailed calculation of the strain in ZnO NWs can be found in the support information of our previously work[1].

The output light emission images were recorded by CCD and the electroluminescence spectra were recorded using a fiber optical spectrometer (Master Systems Felix32 PTI). We monitored the pressure change from the light emitting intensity change with image acquisition and processing technologies.

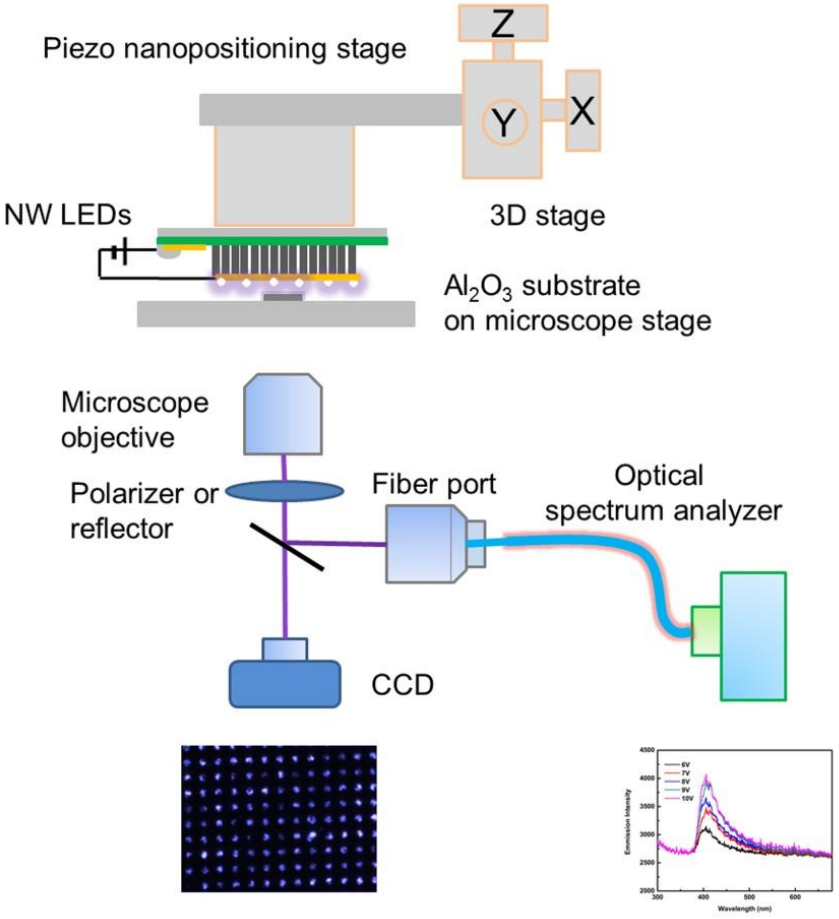

Figure S1 | Schematic diagram of the measurement system for characterizing the performance of a ZnO nanowire LEDs under applied compressive strain.

B: FEM modeling of basic mechanics and performance of the device

To carry out a systematical study about the device's performace, we build a FEM modeling using COMOSOL (version 4.2a) and studied the device response based on models conducted with different geometry (NWs diameter, NWs length, NWs spacing), different material properties (Young's modulus, substrate thickness and modulus). All of the parameters of the structure layouts in the FEM modeling are the same as for practical devices. Some design rules are derived through this systematical FEM modeling for achieving optimum performance.

B1. Several design rules derived from FEM modeling

We have carried out a systematically FEM modeling of the device response, as presented in the next few subsections, for different NW geometry (diameters and length), NW spacing, matrix modulus, substrate thickness and modulus. Based on the numerical calculations, several design rules are derived as summarized as follows:

(1) The device is very uniform, the distribution of stress and strain in the ZnO NWs are very uniform over 99.7% for a 2cm*2cm device used in our experiment, only the 30 μm at the edge zone is not very uniform (Fig. S2 and S3)
(2) The length of ZnO NWs is not very important for the device when the length is less than 25 μm, which approaches the limitation of the NW length fabricated by hydrothermal methods. (Fig. S4)
(3) Spacing is very important for the device, and there is an optimum spacing when the diameter of the NWs is fixed. For NWs with diameter about 1.5 μm, the best spacing is 8 μm. (Fig. S5)
(4) The diameter of ZnO NW is very important to the performance of the device. Small diameter would have good response and good sensitivity. Ideally, we will try to use small diameter ZnO NWs, such as 100 nm. However, by considering the fabrication cost and the device performance, 1 μm is a good choice. (Fig. S6)
(5) For the matrix materials, it is better to use the one with smaller modulus. By considering the electronic property, and micro-fabrication related issues, PMMA and BCB are two best choices. (Fig. S7)
(6) Thickness and modulus of the substrate are not important for our common substrates, such as sapphire and silicon wafers. By considering the ZnO NW growth condition and the LED technology, sapphire is the best choice for our experiment. (Fig. S8 and S9)
(7) A tiny fluctuation (e.g. 1-2%) in the length of NWs does not affect the sensing result after depositing the top ITO electrode and the packaging layer, because the large deformation of the ITO and packaging layer due to their low young's modulus will tolerate the small variation in NW lengths (Fig. S10)

B2. Distribution of strain and stress in the device for different nanowire dimensions.

As shown in Fig. S2, 51 ZnO NWs array were built on a GaN/Sapphire substrate, the matrix is PMMA as we used in the experiments, and a layer of 300 nm ITO layer is on top of the composite structure. At last, a layer of 5 μm PDMS is on the top most of the structure. There are two reasons for introducing the PDMS layer, one is to serve as the package layer, and the other is the convex character pattern of "PIEZO" made by polymer (SU-8), where the stress was applied to.

The dimensions of each component are as following:

Sapphire substrate: thickness = 20 μm (this thickness will NOT affect the performance of the device, see Fig. S8)

ZnO NWs: diameter = 1.5 μm, length = 3.8 μm (the average in our experiments)

ZnO NW spacing: 4 μm (the center to center distance between two adjacent ZnO NWs)

PMMA: 2.5 μm by 3.8 μm

ITO top electrode: 300 nm

PDMS layer: 5 μm

After a uniform stress of 0.8 GPa is applied on the surface of the device, the stress distribution in the devices is shown in Fig. S2a. Due to the limitation of our computation power, we only built 51 NWs on the substrate in this modeling, it is clearly that the stress distribution in ZnO NWs is very uniform over the central 200 μm (see the enlarged result in Fig. S2b and Fig. S2c), except the four ZnO NWs at the edges, which is only less than 20 μm, as shown in Fig. S2a.

For the devices used in the test, the size is about 2 cm by 2 cm, the response of NWs of the device can be treated as very uniform if we build the strain sensor on the center part of the whole device, not at the 100 μm edge area.

To further confirm the uniformity of stress in ZnO NWs, we extract the stress profile at the interface between n-ZnO and p-GaN, where the light emit, and shown in Fig. S3c and Fig. S3d. we can find that the stress in ZnO NW is very uniform and is about 1.7GPa (Fig. S3c); the strain in ZnO is also very uniform, which is near 1.0% (Fig. S3d).

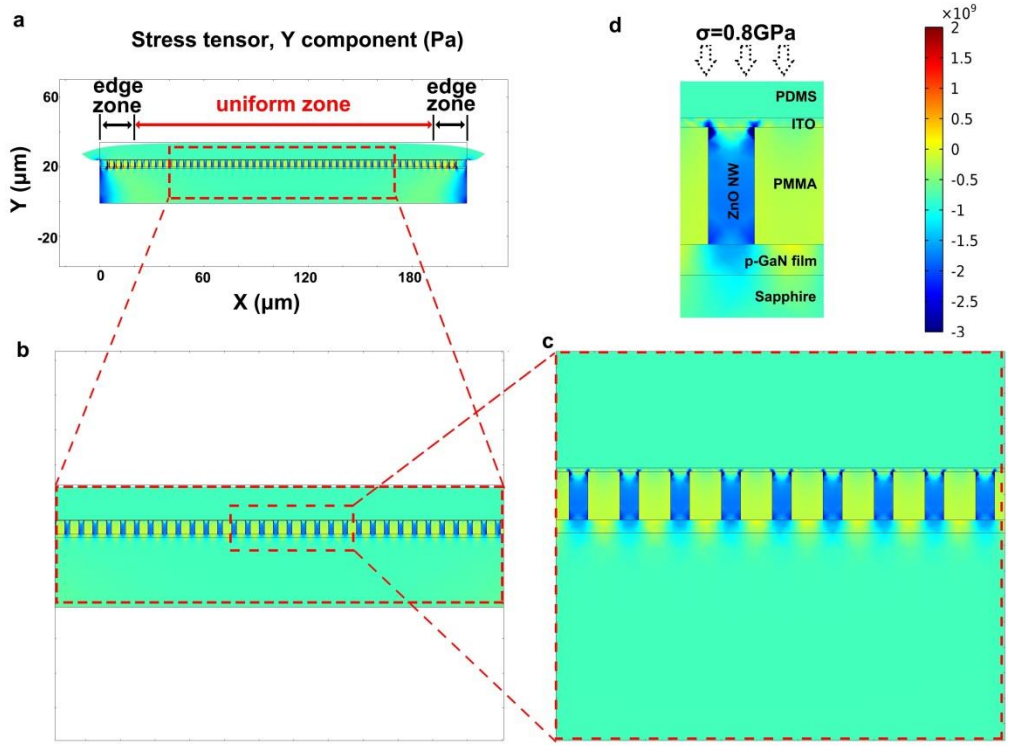

Figure S2 | FEM modeling shows the distribution of stress in the device. a, A low-magnification view of the device. **b-c,** Enlarged view of the device, indicating that the stress is uniform in the middle of the device. **d,** The stress in a single ZnO NW, and the scale bar of stress, which unit is Pa.

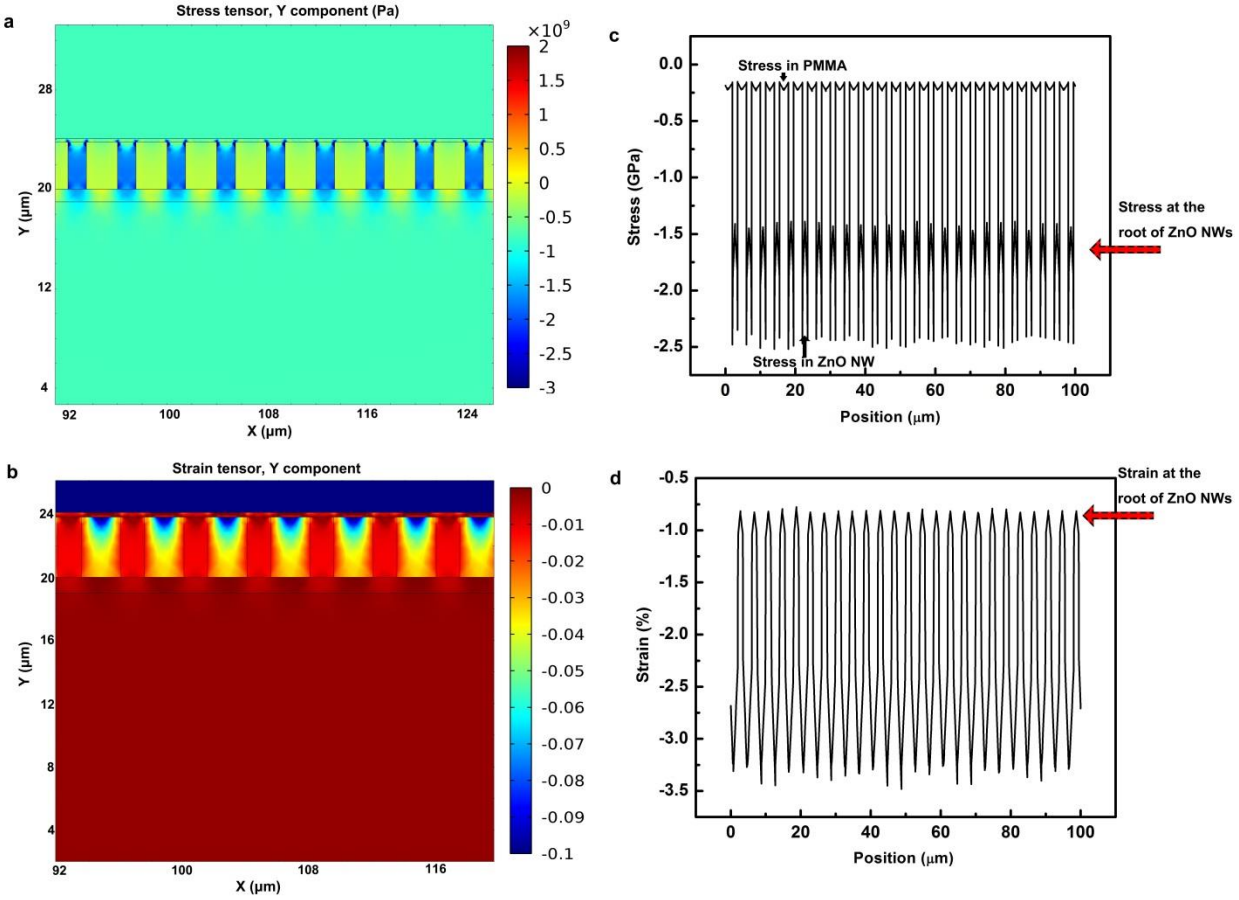

Figure S3 | a, The stress distribution in the device. **b,** The strain distribution in the device. **c,** The 1D cut profile of the stress at the interface between ZnO and GaN. **d,** The corresponding 1D cut profile of the strain at the interface between ZnO and GaN.

B3. Effect of NW diameter, length and spacing on device performance

As shown in Fig. S4, three different NW lengths are used in the FEM modeling, 3.8 μm, 15 μm and 25 μm. The results of the NWs with length 3.8 μm and 15 μm are shown in Fig. S4a and S4b, and the 1D cut profile of stress and strain at the interface between ZnO and GaN is extracted and presented in Fig. S4d and S4e. We can reach the conclusion from the line profile that the length of the ZnO NWs DOES NOT affect the stress and strain distribution in ZnO NWs, which decides the performance of the device; it will only change the stress and strain distribution in the matrix (PMMA), which will not have impact on the performance of the device and the intensity of LEDs.

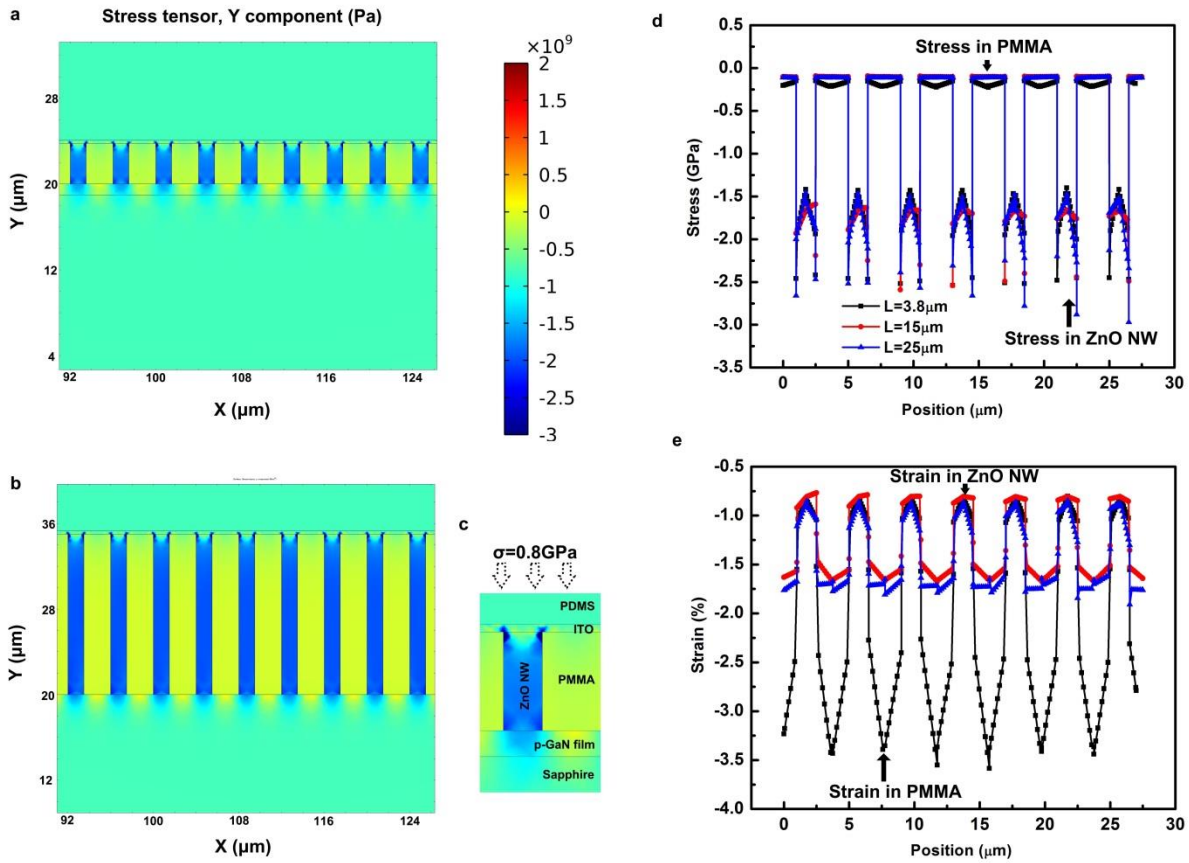

Figure S4 | The FEM modeling results showing the stress and strain distribution depending on the length of NWs. a, The length of ZnO NW is 3.8 μm. **b,** The length of ZnO NW is15 μm. **c,** The stress in an individual ZnO NW. **d-e,** The 1D cut profile of stress and strain at the interface between ZnO and GaN.

The spacing effect was modeled with all other parameters being fixed, and the results are shown in Fig. S5. Here we define spacing as the NW center to center distance. We set the spacing as 4 μm, 6 μm, 8 μm, 10 μm and 12 μm, and three of them are shown in Fig. S5a (4 μm), Fig. S5b (8 μm), and Fig. S5c (12 μm). The line profile of the stress at the interface between ZnO NW and GaN film is shown in Fig. S5d. There exists an optimum spacing value for the sensitivity of the device; the stress is larger at the root of ZnO NWs in case of the spacing of 8 μm than that of spacing 4 μm and 12 μm, when an external stress about 0.8 GPa is applied on the surface of the device as shown in Fig. S5c.

The plots of the stress at the root of ZnO NW and the PMMA versus the spacing are presented in Fig. S5e. At the beginning, the stress in the ZnO increases when the spacing increases. This is because the density of ZnO NW decreases, so the stress in each NW increases. When the spacing continues to increase, the stress in the ZnO NW begins to decrease when the spacing is over 8 μm (see the blue plot in Fig. S5e). This is because a part of the external stress was applied on the PMMA matrix, which is approved by the FEM modeling result shown in Fig. S5e, red line. We can see that the stress in the PMMA increases with increasing the spacing. We can reach a conclusion that an optimum spacing exists for our device, 8 μm is the best spacing for the device with NWs of diameter 1.5 μm, which was used in our experiment and this FEM modeling.

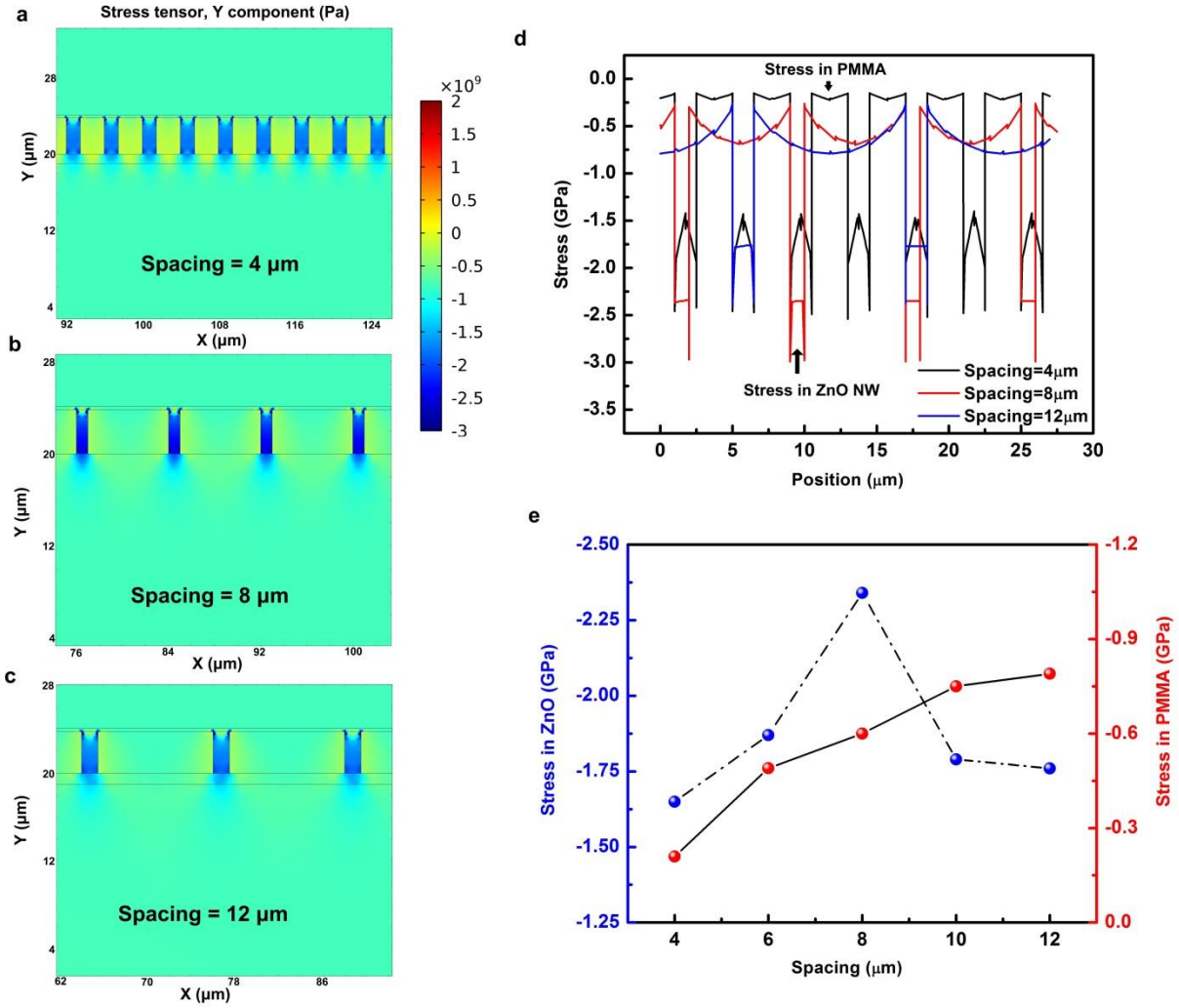

Figure S5 | The FEM modeling results showing the stress distribution depends on the spacing of NWs. a-c, The spacing of the NWs is 4 μm, 8 μm and 12 μm, respectively. **d,** The 1D cut profile of stress at the interface between ZnO and GaN, when the devices have different spacings, the data were extracted from (a-c). **e,** The maximum stress in the root of ZnO NW (blue) and PMMA (red) versus different spacings.

The relationship between the NW diameter and the device sensitivity was carried out with the FEM modeling as well. All other parameters are fixed except the NW diameter, and the results are shown in Fig. S6. Three typical FEM modeling results are shown in Fig. S6a (diameter 0.5 μm), Fig. S6b (diameter 1.5 μm) and Fig. S6c (2.5 μm), which obviously shows higher stress in the device with smaller diameter NWs. And the 1D cut profile of stress at the interface between ZnO and GaN are extracted and presented in Fig. S6d. Fig. S6e shows the relationship between the NW diameter and the stress in the ZnO NW.

These results indicate that, the smaller the NW diameter is, the higher stress in the ZnO NW, which means the intensity of the LED is brighter, and better sensitivity of the devices will be obtained. However, in the fabrication process, there are several limitations for growth small diameter ZnO NWs. First, a photoresist layer with patterned pore diameter about 800 -1500nm was prepared by photolithography (PL),

which makes the NW diameter around 1 μm. If we choose electron beam lithography (EBL), we can reach NW diameter about 200-300 nm or even less than this, as reported by us previously (Adv. Mater. 10, 22(42), 4749). Based on considering the cost and the device performance, the diameter used in our experiment is around 1-1.5 μm.

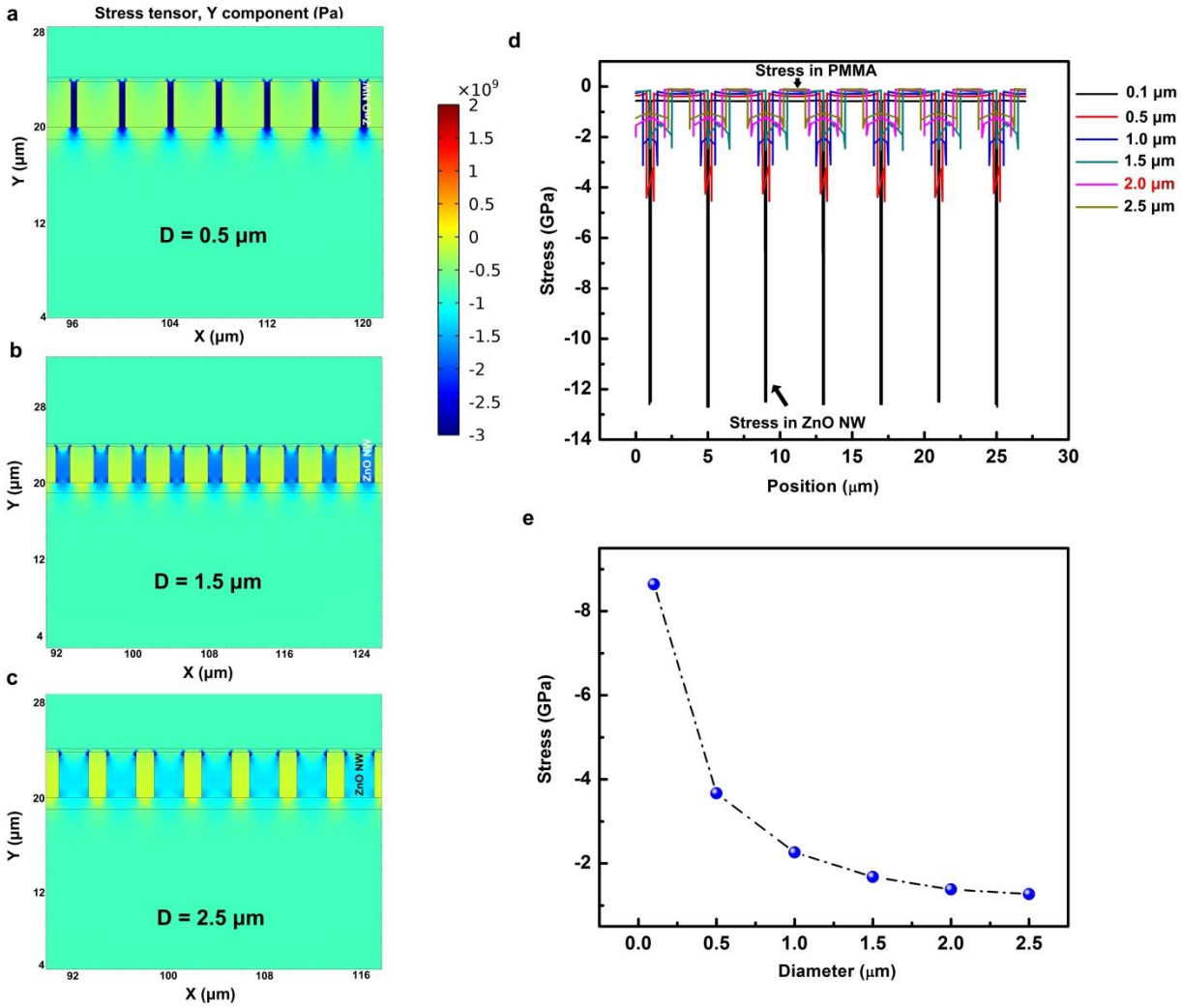

Figure S6 | The relationship between the NW diameter and the device sensitivity. Three typical diameter (a) 0.5 μm, (b) 1.5 μm, (c) 2.5 μm. **d,** 1D cut profile of stress at the interface between ZnO and GaN. **e,** Relationship between the NW diameter and the stress in the ZnO NW.

B4. Effect of the modulus of the matrix material

The modulus of the matrix material was studied with the FEM modeling, two kinds of frequently used matrix materials, PMMA (modulus 3 GPa, see Fig. S7b) and Benzocyclobutene (BCB, modulus 3.2 GPa), two other hypothetical matrix materials with modulus 1GPa (Fig. S7a) and 10 GPa (Fig. S7c) are used for the simulation, all other parameters are fixed, and the results are shown in Fig. S7.

We can found that the stress in ZnO NW decrease when the matrix modulus increases, which means the sensitivity of the LED devices decreases with increasing the matrix modulus (Fig. S7d-e).

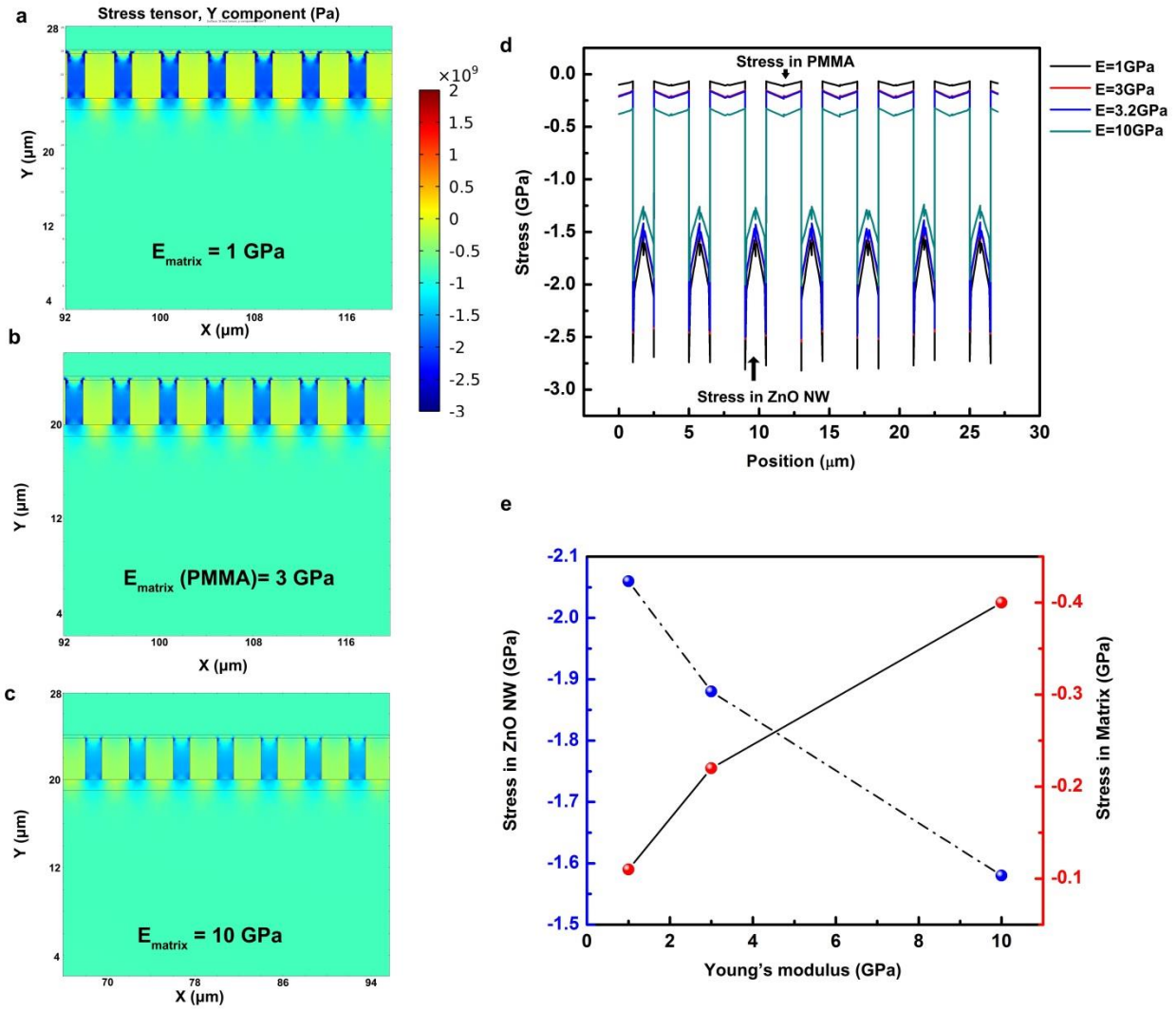

Figure S7 | The FEM modeling results showing the stress distribution depends on the modulus of matrix. a-c, The stress distribution depends on the modulus of matrix, with matrix modulus 1 GPa (a), 3 GPa (b) and 10 GPa (c), respectively. **d,** The 1D cut profile of stress at the interface between ZnO and GaN, with different matrix modulus. **e,** Plots show the relationship of the maximum stress at the root of ZnO NWs and the matrix with the young's modulus of different matrix.

B5. Effect of modulus/thickness of the substrate

The thickness and the modulus of the substrate are not important to the device, the FEM modeling results are shown in Fig. S8 and Fig. S9.

We can found that the stress distribution in the device remains the same when the substrate thickness changes from 20 μm, 100 μm to 200 μm (see Fig. S8).

Single crystal silicon wafer was chosen as the substrate besides sapphire, we can see that the stress distribution in the device is the same (see Fig. S9).

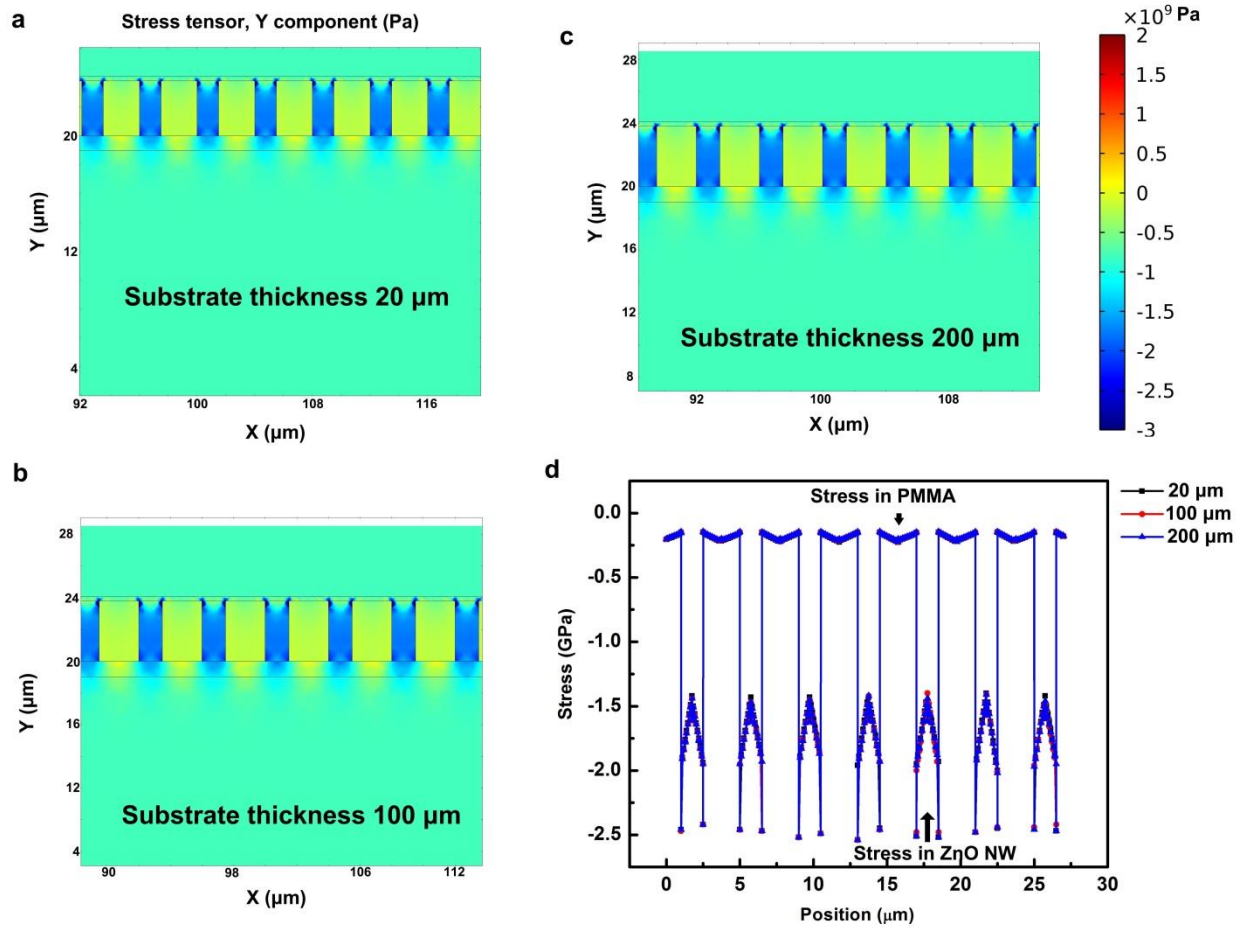

Figure S8 | The effect of the substrate thickness on the stress distribution in the devices. a-c, The substrate thickness is 20 μm, 100 μm and 200 μm, respectively. **d,** The 1D cut profile of stress at the interface between ZnO and GaN, with different substrate thicknesses.

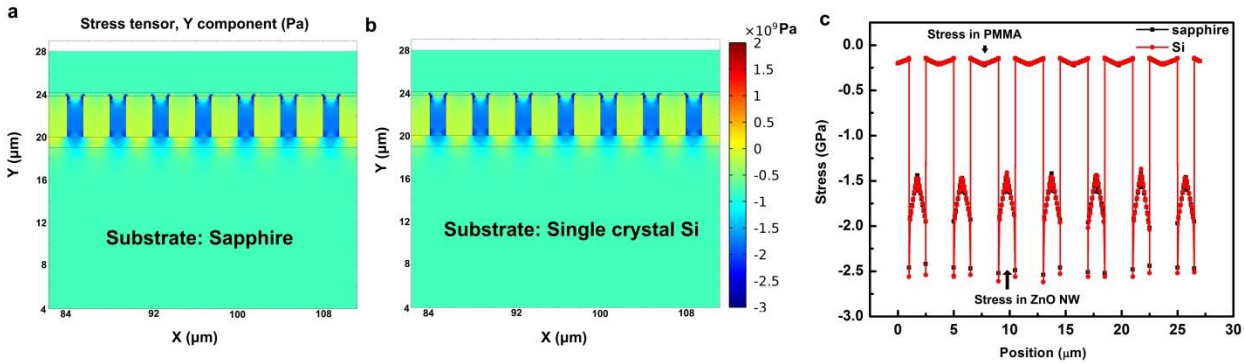

Figure S9 | The effect of the substrate modulus on the stress distribution in the devices. a, Using sapphire as the substrate. **b,** Using single crystal Si wafer as the substrate. **c,** The 1D cut profile of stress at the interface between ZnO and GaN, with different substrate modulus.

B6. Effect of length variation of the NWs

The length control is challenging in practical nanowire synthesis. The best we can do is a fluctuation of.1%-0.15%. A small fluctuation in the length of the nanowires is not an issue for the device performance, because we can use the thickness modulation of the top electrode as well as the top packaging materials (PDMS polymer) to tolerate the small various in nanowire length. In such a case, even there is a small variation in the nanowire length, the result will not be affected.

A FEM modeling was carried out and the results are shown in Fig. S10. In this modeling, 1% fluctuation of NWs length was set in the middle NW in Fig. S10b (1% longer) and Fig. S10c (1% shorter). The stress distributions in ZnO NWs of each case are the same for all of the cases. To see more clearly, a line profile of stress and strain distribution at the root of ZnO NWs are presented as Fig. S10e and S10f. We can find that 1% fluctuation of length does not have any influence to the stress and strain response in ZnO NWs. This means, after being modulated of the top electrode as well as the top packaging materials, 1% length fluctuation will not affect the device performance.

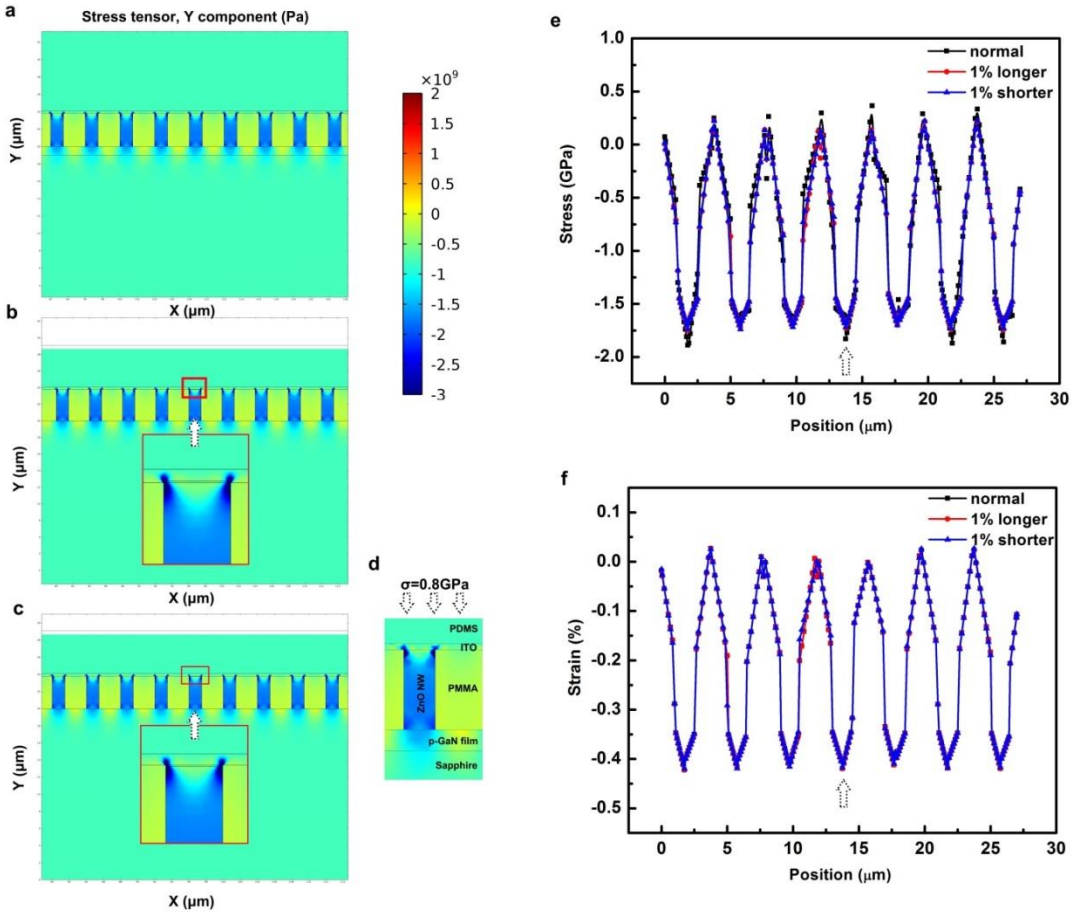

Figure S10 | The effect of the length fluctuation of NWs length on the stress distribution in the devices. a, The length of all the NWs are the same. **b,** The length of the middle NW is 1% longer than others. **c,** The length of the middle NW is 1% shorter than others. **d-e,** The 1D cut profile of stress and strain at the interface between ZnO and GaN. The NW with length fluctuation was marked with an arrow.

C: Devices fabrication process and hydrothermal growth method

C1. Hydrothermal growth method

A p-type 2 μm GaN film on *c* plane sapphire fabricated by metal organic chemical vapor deposition (MOCVD) was used in the experiment. On which, a 500 nm thick SU-8 (from MICROCHEM) photoresist layer, with patterned pore diameter about 800 nm and 4 μm pitch, was prepared by photolithography (PL). Subsequently, the substrate with patterned SU-8 was then put into the nutrient solution, containing 15-50 mM zinc nitride (Alfa Aesar) and 15-50 mM hexamethylenetetramine (HMTA) (Fluka), for NWs growth at 95 ℃ for 3 h in an oven. Notably, ZnO NWs can be grown with a broad concentration variation of the nutrient solution, from 5mM to 100mM. The concentration of the nutrient solution will control the growth speed, NWs' length and diameter. ZnO NWs grew at the GaN sites exposed to the solution, and uniformly patterned ZnO NW arrays were hence obtained in a scale of centimeters.

C2. Fabrication process of a piezoelectric nano-LED array (Fig. S11):

(1) a 500 nm thick SU-8 photoresist layer was spun coated onto the GaN/Sapphire substrate,
(2) a photolithography process was carried out, obtained a pattern with pore diameter about 800 nm and 4 μm pitch
(3) Put the patterned the GaN/Sapphire substrate into the nutrient solution, containing 15-50 mM zinc nitride and 15-50 mM HMTA, at 95 ℃ for 3 h in an oven.
(4) A layer of PMMA was spun coated to wrap around the ZnO NWs.
(5) Then oxygen plasma was applied to etch away the top part of the PMMA, exposing the tips of the NWs.
(6) A 10-nm by 100-nm layers of Ni/Au were deposited by electron beam evaporation onto the p-GaN followed by rapid thermal annealing in air at 500 ℃ for 5 min.
(7) A 100-300 nm ITO film was sputtered as the top common electrode of the entire NWs.
Here, the fabrication of the bottom and top common electrodes are not limited to be at last, the Ni/Au electrode was deposited before the growth of ZnO NWs as well.

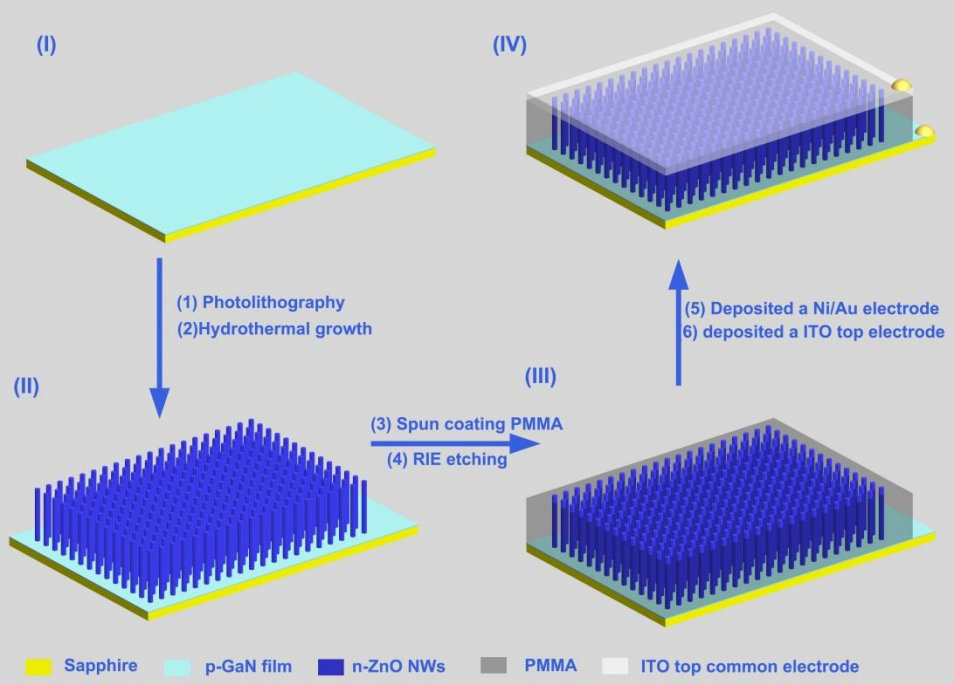

Figure S11 | The fabrication process of the piezoelectric nano-LED array.

D: I-V characterization and electroluminescence images of nano-LEDs array

Before the electromechanical and optical measurements, the original optoelectronic performance of the nano-LED array without strain was measured first. The current-voltage (*I*-*V*) characteristic of an LED device is shown in Fig. S12. The *I*-*V* curve clearly shows a nonlinear increase of current under the forward bias, which indicates reasonable *p*–*n* junction characteristics and the possibility of light emission.

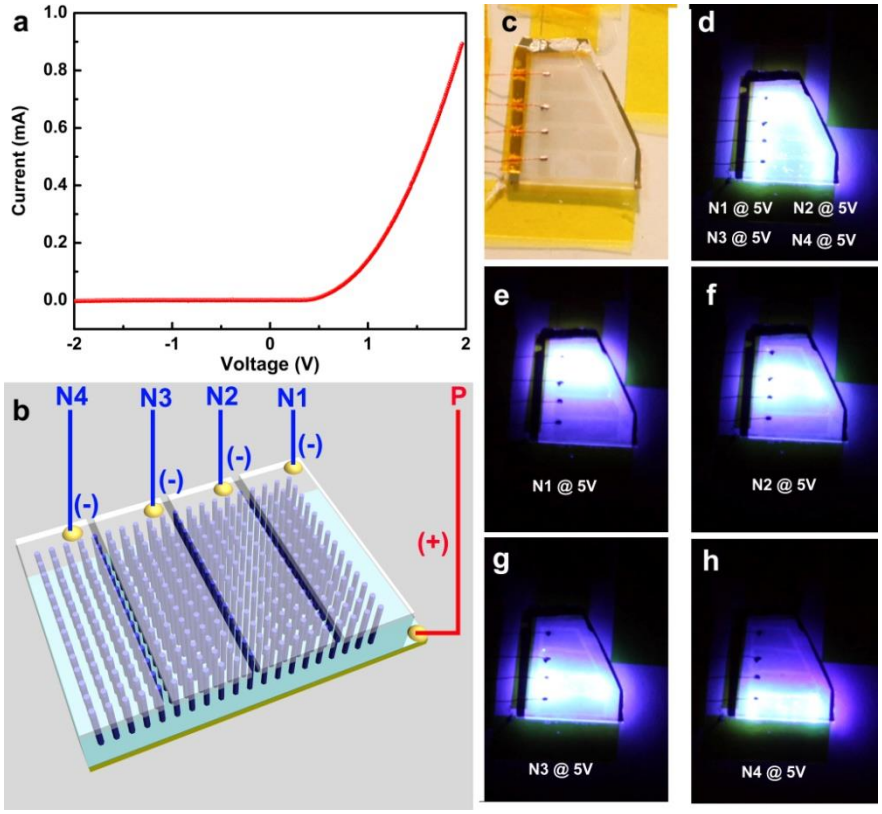

Figure S12 | I-V characteristics and electroluminescence images of nano-LEDs array. a, I-V characteristics of the device at forward bias without strain. **b,** Schematic image of a LEDs device consisting of four negative electrodes, noted as N1, N2, N3 and N4. **c,** Optical image of this four negative electrodes device. **d-h,** The corresponding image when the device was electrically light up at a bias voltage of 5 V. **d,** all the four negative electrodes were at 5 V; **e,** N1 at 5 V; **f,** N2 at 5 V; **g,** N3 at 5 V; and **h,** N4 at 5V , showing a blue-white light emission from the NW LED array.

E: Repeatability test and reversible experiments

E1: 25 repetitive "on-off" cycles of applying pressure on 10 far-separated NW LEDs

The stability and reproducibility of the NW LED sensor array is studied by examined light emitting intensity of individual-pixels when they are under a -0.0186% strain for 25 repetitive "on-off" cycles of applying pressure. To exclude the crosstalk from the adjacent pixels, a device consisting of sparsely distributed NW LEDs, which are numbered as 1-10, is used in this study (Fig. S13a). The average enhancement factors of these ten nano-LED devices are about 15-20% under -0.0186% strain (see table S1). The average fluctuation of the *E* factor of these 10 nano-LEDs is less than ±7%, much smaller than the signal level presented in Fig. 3e. Further, for the pixels we have studied, the change in *E* factor shows no specific trend or synchronized pattern when the device is repeatedly compressed (Fig. S13b and Fig. S14), indicating that the observed enhancement in light emission is dominated by the effect from piezoelectric charges at the ends of the NWs, rather than a change in contact-area at the ZnO-GaN junction/interface, because a change in contact area would result in a synchronized change of the *E* factors for all of the NW LEDs during cycled mechanical straining.

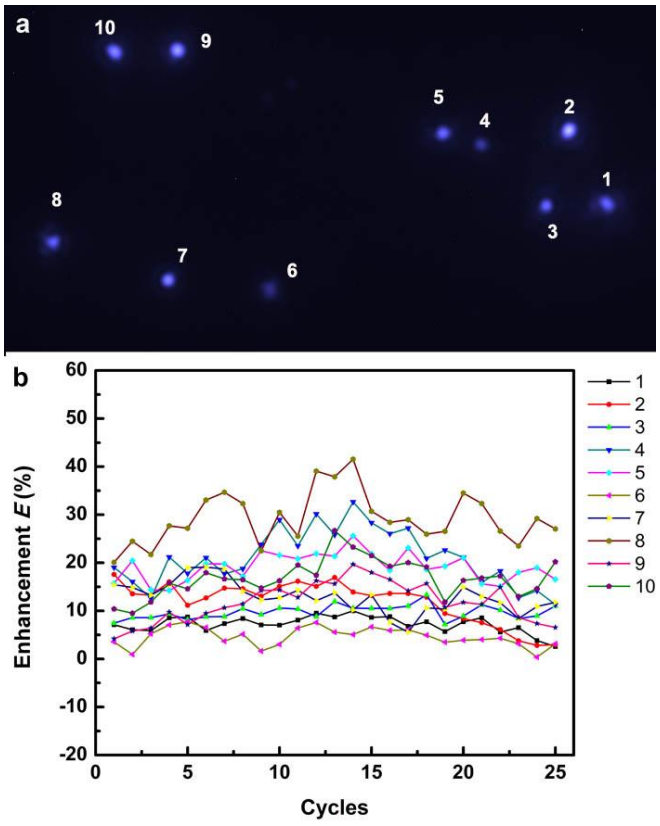

Figure S13 | Repetitive "on-off" cycles of applying pressure on 10 far-separated NW LEDs. a, Electroluminescence images of 10 ZnO NW LEDs, which are marked as 1 to 10. **b,** The enhancement *E*

factor of these 10 nano-LEDs when they were repeatedly strained to -0.0186% strain for 25 "on-off" cycles, showing a good reproducibility in the LED intensity. Detailed data of the *E* factor is listed in the following Table S1 and Fig. S14.

Table S1. The enhancement factors of the 10 nano-LEDs under a strain of -0.0186% in the 25 cycles.

Samples / Cycles	#1	#2	#3	#4	#5	#6	#7	#8	#9	#10
1	7.10	17.57	7.44	19.03	15.76	3.54	15.43	20.09	4.20	10.38
2	6.06	13.55	8.59	16.06	20.43	0.92	14.88	24.49	5.79	9.50
3	5.87	13.25	8.59	12.58	14.38	5.21	13.24	21.74	6.40	11.82
4	8.53	16.02	9.35	21.18	14.23	7.06	15.40	27.68	9.75	15.75
5	8.73	11.17	8.16	17.77	16.37	7.72	18.97	27.18	7.13	14.57
6	5.91	12.68	8.73	21.06	19.78	6.54	19.08	33.05	9.47	17.92
7	7.34	14.73	8.82	17.70	19.78	3.66	18.70	34.66	10.65	16.63
8	8.40	14.58	10.48	18.74	17.20	5.13	14.07	32.33	11.43	16.47
9	7.07	13.07	9.23	23.83	22.52	1.63	12.27	22.49	14.22	14.75
10	7.01	15.09	10.58	28.96	21.57	3.01	12.70	30.49	14.35	16.24
11	8.06	16.15	10.38	23.51	20.85	6.43	14.26	25.54	12.79	19.50
12	9.52	15.09	8.78	30.15	21.89	7.59	12.11	39.08	16.27	17.41
13	8.71	16.93	11.94	25.82	21.37	5.56	13.74	37.89	15.60	26.69
14	9.98	13.90	10.54	32.67	25.63	5.05	10.19	41.55	19.67	23.25
15	8.62	13.15	10.51	28.33	21.82	6.66	13.33	30.72	17.98	21.48
16	8.80	13.62	10.51	26.05	18.43	5.90	7.56	28.42	16.52	19.28
17	6.78	13.62	10.99	27.20	23.09	6.07	5.56	28.96	14.17	20.02
18	7.72	12.87	13.34	20.91	18.62	4.93	10.63	25.97	15.68	19.11
19	5.67	9.44	7.17	22.61	19.28	3.46	10.36	26.54	10.71	11.78
20	7.72	8.38	8.92	21.11	21.04	3.87	14.90	34.50	11.77	16.33
21	8.53	7.54	11.26	15.94	15.62	4.01	13.00	32.32	11.33	16.81
22	5.57	6.11	10.15	18.27	15.10	4.28	11.68	26.60	14.92	17.25
23	6.50	3.77	8.41	12.69	18.00	3.16	8.41	23.50	8.63	12.98
24	3.80	2.82	8.95	14.21	18.96	0.35	10.90	29.20	7.36	14.59
25	2.56	2.94	11.02	11.30	16.56	3.14	11.78	27.06	6.54	20.18
Average Enhancement (%)	7.22	11.92	9.71	21.11	19.13	4.59	12.93	29.28	11.73	16.83

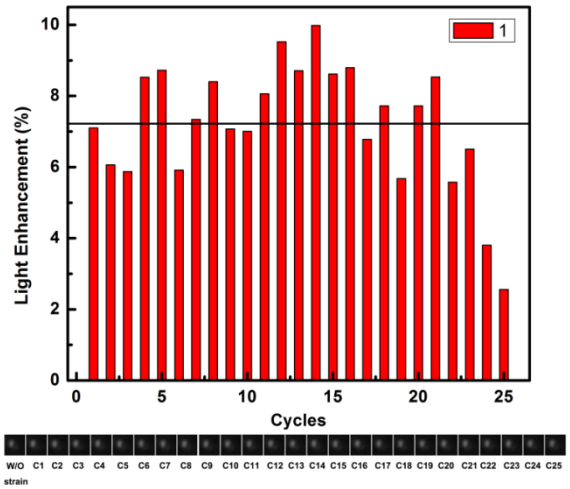
1
Light Enhancement (%)
Cycles
W/O C1 C2 C3 C4 C5 C6 C7 C8 C9 C10 C11 C12 C13 C14 C15 C16 C17 C18 C19 C20 C21 C22 C23 C24 C25
strain

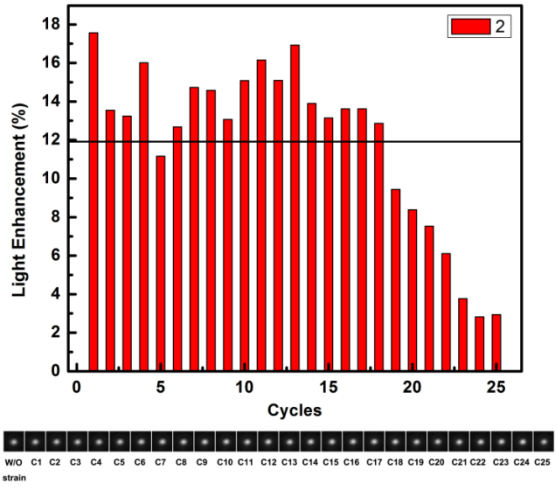
2
Light Enhancement (%)
Cycles
W/O C1 C2 C3 C4 C5 C6 C7 C8 C9 C10 C11 C12 C13 C14 C15 C16 C17 C18 C19 C20 C21 C22 C23 C24 C25
strain

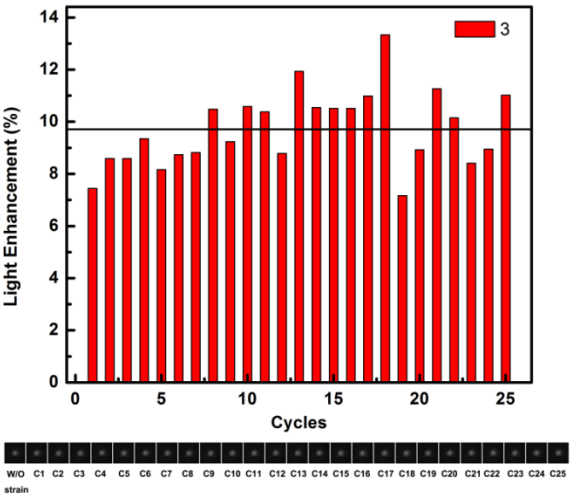
3
Light Enhancement (%)
Cycles
W/O C1 C2 C3 C4 C5 C6 C7 C8 C9 C10 C11 C12 C13 C14 C15 C16 C17 C18 C19 C20 C21 C22 C23 C24 C25
strain

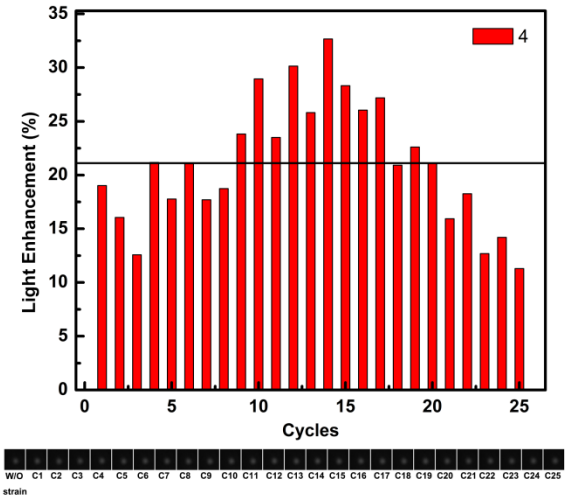
4
Light Enhancement (%)
Cycles
W/O C1 C2 C3 C4 C5 C6 C7 C8 C9 C10 C11 C12 C13 C14 C15 C16 C17 C18 C19 C20 C21 C22 C23 C24 C25
strain

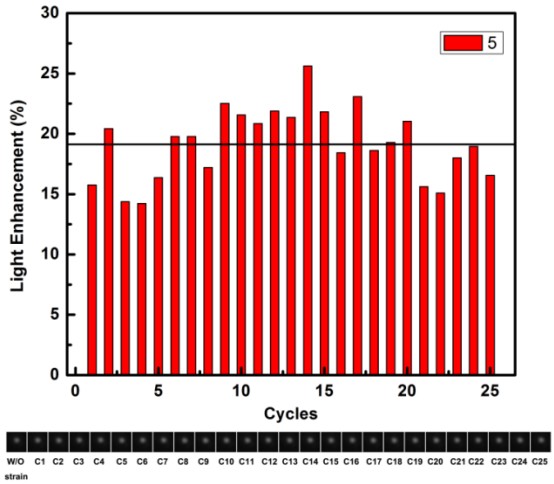
5
Light Enhancement (%)
Cycles
W/O C1 C2 C3 C4 C5 C6 C7 C8 C9 C10 C11 C12 C13 C14 C15 C16 C17 C18 C19 C20 C21 C22 C23 C24 C25
strain

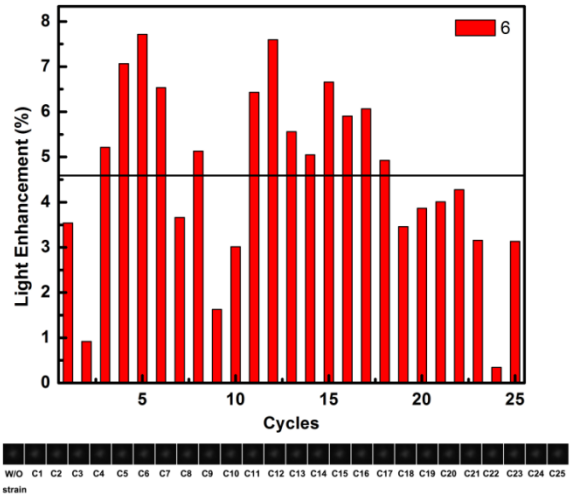
6
Light Enhancement (%)
Cycles
W/O C1 C2 C3 C4 C5 C6 C7 C8 C9 C10 C11 C12 C13 C14 C15 C16 C17 C18 C19 C20 C21 C22 C23 C24 C25
strain

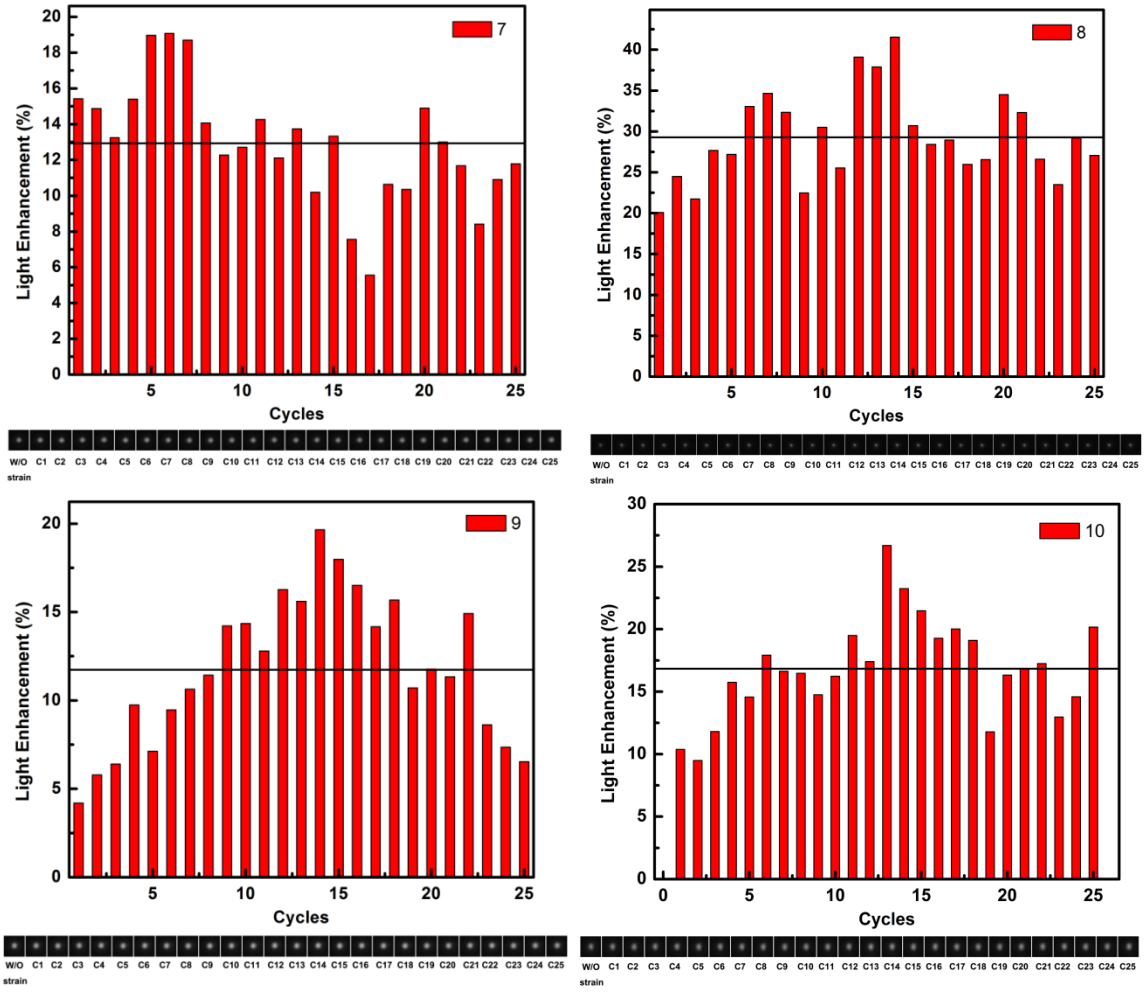

Figure S14 | The enhancement *E* factors of these 10 nano-LEDs when they were repeatedly strained to -0.0186% for 25 "on-off" cycles. The nano-LED numbered 8 is the one shown in Fig. 3f.

E2: repetitive "on-off" cycles of applying pressure on NW LEDs arrays, consisting of over 20,000 NW LED pixels.

We add more solid data in the revised version, which proves that our devices have excellent stability, repeatability and reversibility. First, we carried out repetitive "on-off" cycles of applying pressure on NW LEDs arrays (Fig. S15). The images unambiguously show that the enhancement in LED intensity occurred apparently at the pixels that were being compressed by the molded pattern, and decreased when the strain was released. The images obviously show that our device has a very good repeatability and stability. It is a great step forward, since there are great challenges when extension devices from single wire to a practical array.

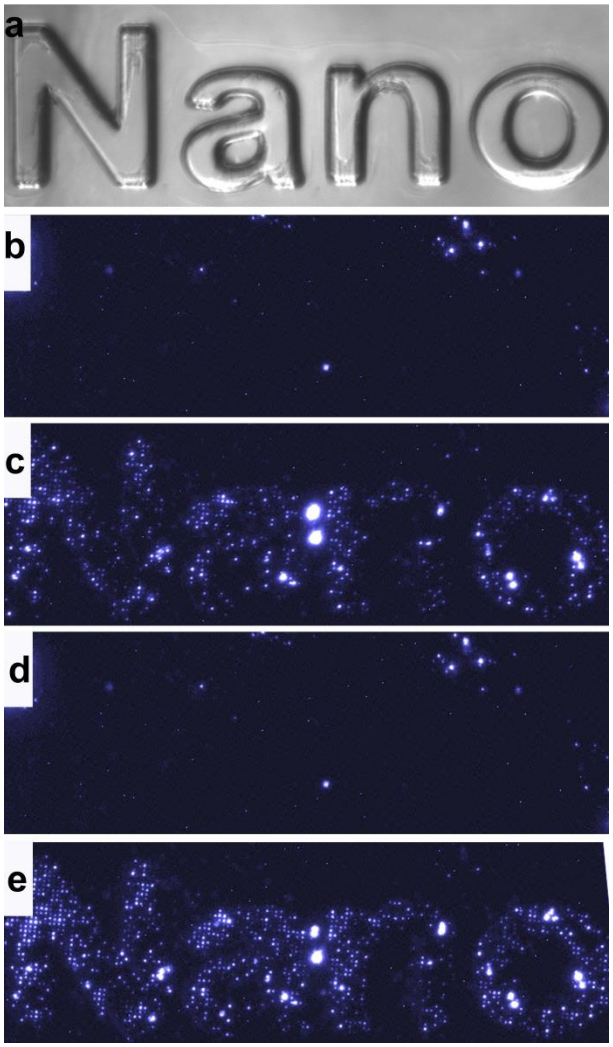

Figure S15 | Repetitive "on-off" cycles of applying pressure on NW LED arrays, consisting of over 20,000 NW LED pixels, showing the repeatability of the nanowire LEDs. The applied voltage was 5 V. **a,** An optical image of a sensor array with a "nano" SU-8 convex mold on the top. **b-e**, Electroluminescence images of the sensor array under 2 cycles of applied strain, without strain (b), strain applied (c), strain released (d) and strain reapplied (e), respectively. The images obviously show that our device has a very good repeatability and stability.

E3: Reversible experiments by applying strain step by step

We carried out a reversible experiment by applying the strain step by step, and then releasing the strain step by step. It is obviously that the light emission intensity increases when the applied strain increases step by step (step 1 to 7 of Fig. S16b), and then decreases when the applied strain releases step by step (step 8 to 14 of Fig. S16c). It shows that our devices have very good reversibility.

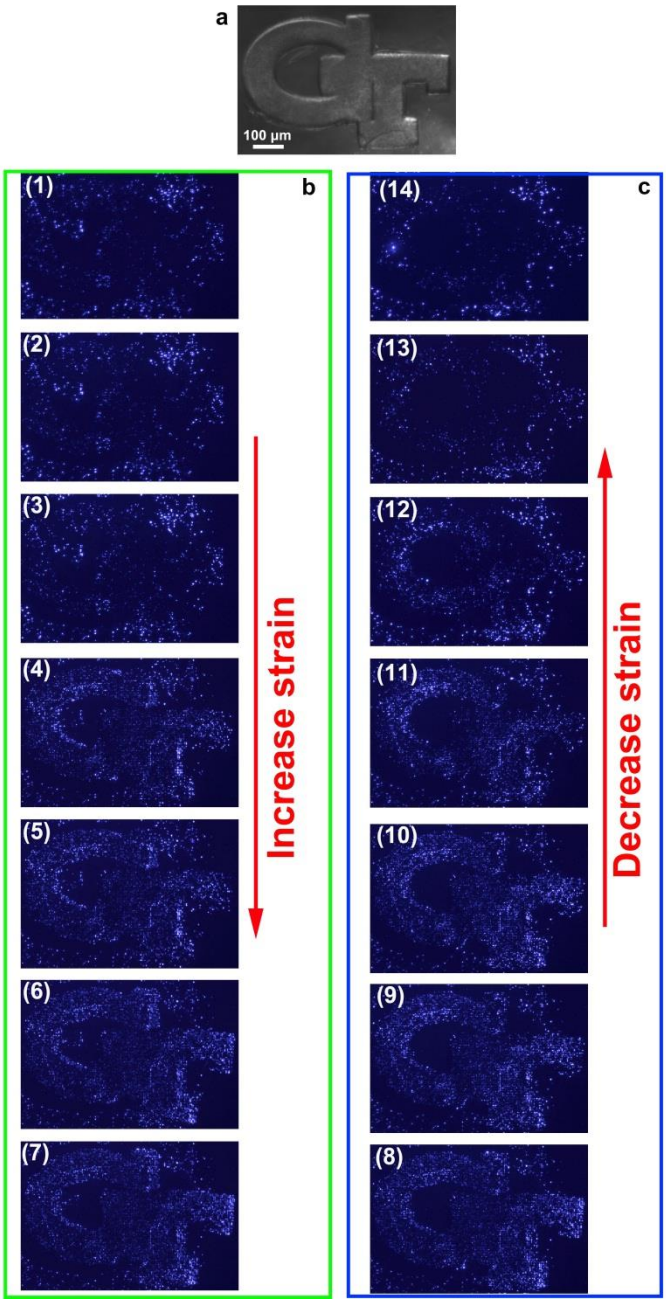

Figure S16 | Reversible experiments by applying strain step by step. The applied voltage was 5 V. **a,** An optical image of a sensor array with a "GT" logo SU-8 convex mold on the top. **b-c,** Electroluminescence images of the sensor array under different strains. The strain was applied on the device step by step (1-7) and then released step by step (8-14). The images obviously show that the enhancement in LED intensity occurred apparently when the applied compressive strain increases, and the enhancement of the LED intensity decreases when the applied strain releases. It shows that our devices have very good reversibility.

F: More High-spatial resolution pressure images supporting Figure 4

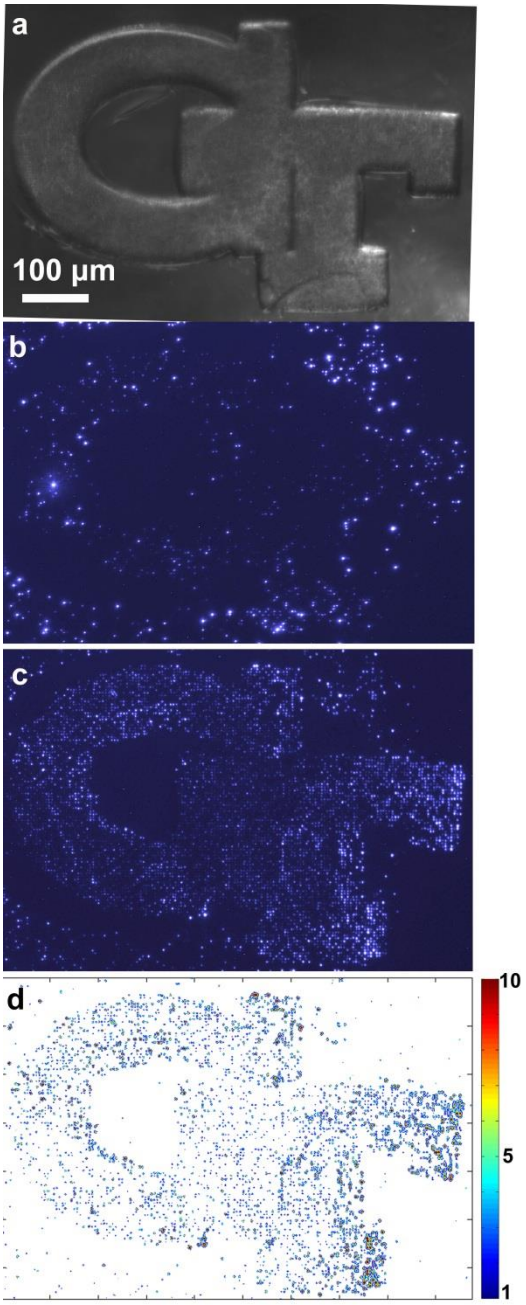

Figure S17 | Another High-spatial resolution pressure imaging of the nano-LED sensor array. The applied voltage was 5 V. **a,** An optical image of a sensor array with a "GT" logo SU-8 convex mold on the top. **b-c,** Electroluminescence images of the sensor array without and with strain, respectively. The images obviously show that the change in LED intensity occurred apparently at the pixels that were compressed by the molded pattern, while those off the molded pattern showed almost no change in LED intensity. **d,** A 2-D contour map of the enhancement factor *E(x,y)* derived from the LED intensity images shown in (b) and (c). It directly presents the logo of Georgia Tech "GT", as fabricated on the mold at the first place.

G. Novel designs for the feasibility to extend the current approach to soft substrates.

There are many potential applications of our strain sensor arrays, such as imaging surfaces, touch pad technology, finger print and imaging, as well as electronic skin, which is the motivation of this work. Although the current study is based on a hard substrate, it is feasible to extend the current approach to soft substrates by several means. Here we just show two of them as examples.

First, with the same device design in the current study, just cut it into small pieces with a size about 500 μm by 500 μm, then transfer these pieces onto a soft substrates and pattern them with a 30-50 μm gap between each, as shown in Figure S18a. By doing so, such device is flexible as shown in Figure S18b and S18c.

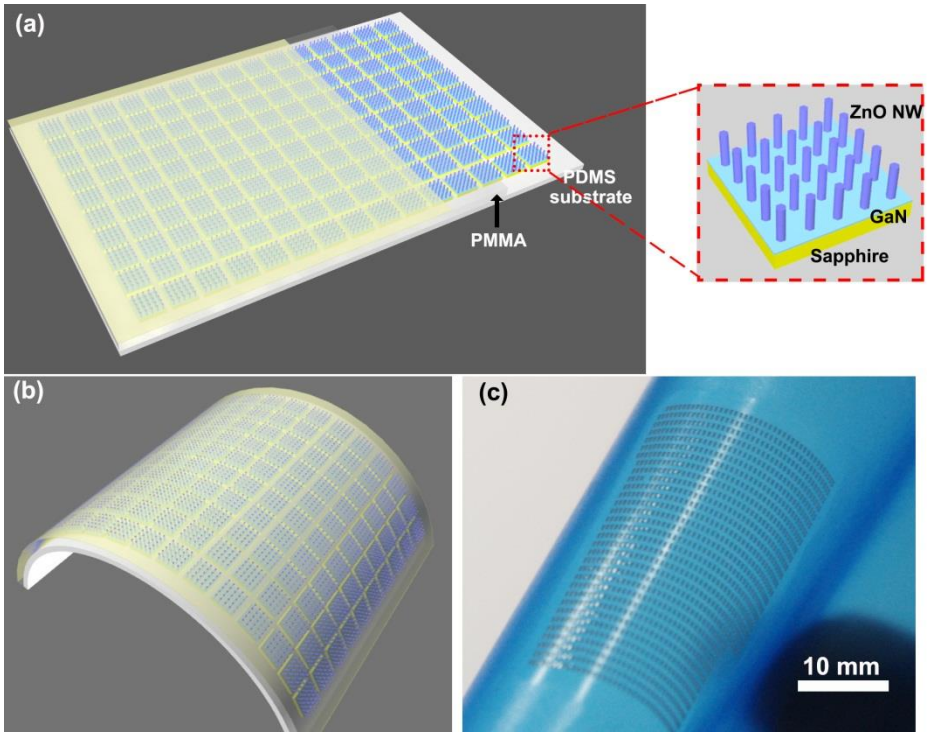

Figure S18 | a, **b**, A new design to show the feasibility to extend the current approach to soft substrates. An enlarged picture of a unit device is presented at the right side. **c**, An optical photo of LEDs array on a PET film showing a good flexibility of such design.

Second, we can also extend current device to other materials, such as ZnO p-n homojunctions. As reported, ZnO NWs can be fabricated on any substrate, including flexible polymers and fibers, fibers and even clothes. In our recent research work, p-type Sb-doping ZnO NWs have been successfully fabricated with hydrothermal method following Dr. Voyles, PM's work (*Nano Lett.* 12, 1331)[2]. These p-ZnO NWs are very stable, and they are still p-type even after 6 months. As designed in Figure S19, such p-ZnO/n-ZnO NWs homojunctions are used for the LEDs array. In such a design, it eliminates the hard GaN and sapphire substrate, and the flexible substrate of the device will greatly broaden the applications of our device.

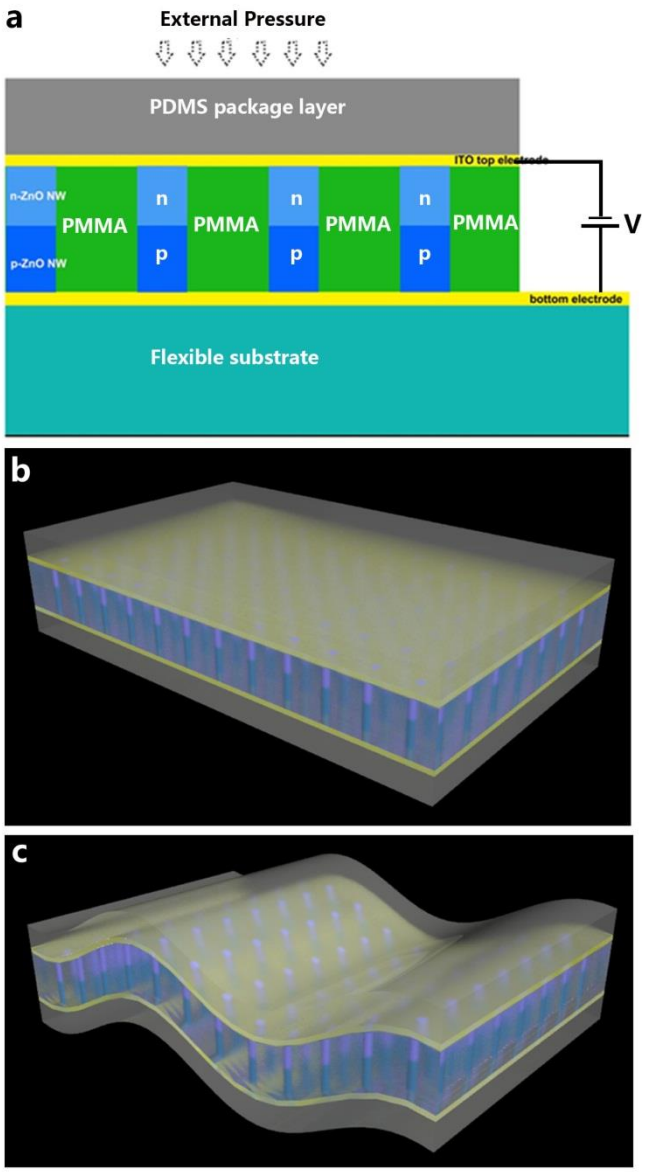

Figure S19 | A novel design shows the feasibility to extend the current approach to soft substrates. The key tech is to use ZnO p-n homojunctions for the LED. **a**, A schematic of the design. **b**, **c**, 3D images demonstrate the flexibility of the device.

Reference:

S1. Yang, Q., Wang, W. H., Xu, S. & Wang, Z. L. Enhancing light emission of ZnO microwire-based diodes by piezo-phototronic effect. *Nano Lett.* **11,** 4012-4017 (2011).

S2. Xia, T. H., Zhang, A. P., Gu, B. B. & Zhu, J. J. Fiber-optic refractive-index sensors based on transmissive and reflective thin-core fiber modal interferometers. *Optics Communications* **283,** 2136-2139 (2010).